Frozen Spin-Wave Structure on the NiO(100) Surface Observed by Metastable He 2^3S Scattering

A. Swan,[1] M. Marynowski,[1] W. Franzen,[1] M. El-Batanouny,[1] and K. M. Martini[2]
[1]*Department of Physics, Boston University, Boston, Massachusetts 02215*
[2]*Department of Physics and Astronomy, University of Massachusetts, Amherst, Massachusetts 01003*
(Received 26 March 1993)

Elastic scattering of metastable 2^3S He has been used for the first time to determine the long-range spin ordering on the surface of an antiferromagnetic insulator. The diffraction pattern obtained from a NiO(100) surface is interpreted as a frozen spin-wave structure in the ⟨10⟩ direction with a period of $6\times a$. The diffraction arises from a spatial variation of the beam attenuation due to scattering from the periodic local spin ordering on the surface and is *not* caused by a spin-spin interaction. The results have been modeled with a modified version of the eikonal approximation using a dissipative, hard, corrugated wall.

PACS numbers: 75.30.Ds, 75.30.Pd, 75.50.Ee, 79.20.Rf

Magnetic ordering in insulating crystals has been the subject of numerous publications over the past several decades. The interest in this topic arises from the existence of several competing mechanisms which tend to produce a rich variety of spin-ordering configurations [1]. It is difficult to predict the predominance of any particular mechanism in a given system *a priori* without the aid of experimental measurements of the spin-ordering configuration. Such measurements have been carried out for the bulk of many crystals using neutron scattering, allowing reasonable theoretical understanding of the competing microscopic mechanisms of magnetic couplings and their relative strengths in many systems to be achieved. In contrast, similar information pertinent to the surfaces of these crystals is almost nonexistent. This is directly attributed to the lack, until now, of an effective probe capable of measuring the surface long-range spin-order configuration. In this paper, it is shown that elastic metastable He 2^3S scattering does provide such a probe and its application to the determination of long-range spin ordering on such surfaces is demonstrated.

In general, when metastable helium atoms strike the surface of a solid, there is an overwhelmingly large probability that they will deexcite to the ground state. The deexcitation may occur via two distinct mechanisms, namely, resonance ionization followed by ion neutralization, or Auger deexcitation [2]. The first of these processes dominates if unoccupied states of the solid are energetically degenerate with the excited He $2s$ electron state: The He $2s$ electron then tunnels into the solid, and the resulting ion is neutralized by a surface electron filling the empty He $1s$ state. The released energy is absorbed by a second surface electron which may escape into the vacuum. In the Auger deexcitation mechanism that operates when resonance tunneling is blocked by a band gap or by filled states in the solid, a surface electron fills the empty He $1s$ state and the excess energy is carried away by ejection of the excited He $2s$ electron. These two deexcitation processes are usually very efficient and characteristically result in a very low survival probability for metastable He atoms ($\sim 10^{-6}$ on metal surfaces) [3]. The large decay probability is utilized in metastable helium atom deexcitation spectroscopy to study electronic properties of surfaces by analysis of the energy distribution of the emitted secondary electrons [4].

However, we recognized that local enhancement of the survival probability of He in its triplet state, He 2^3S (He*), can be achieved when an appropriately located electron energy gap and localized spins are present on the surface [5]. The local nature of the atom-surface interaction together with Auger selection rules may prevent the decay of a He* atom with spin orientation parallel to local surface electron spins as a consequence of the Pauli exclusion principle [5]. (Spin-flip processes are excluded by the short interaction time.) *The survival probability is therefore spin dependent.* A periodic arrangement of the orientations of the local moments on the surface leads to a periodic modulation of the beam attenuation that is reflected in the corresponding diffraction pattern of the elastically scattered He* atoms. Thus diffractive He* scattering reflects not only the geometric surface structure, but also the surface spin ordering through the spin-dependent beam attenuation.

We report here experimental results obtained with our metastable He beam scattering facility. The experimental apparatus consists of a metastable He beam generator and a UHV scattering chamber. The former comprises a nozzle-skimmer assembly that generates a high-intensity, monochromatic He beam, followed by a metastable atom exciter, incorporating an electron gun tuned to the triplet $2s$ state excitation energy. The coaxial geometry of the electron and atomic beams allows a choice between two He* wave vectors, $k_i = 13.6$ Å^{-1} or $k_i = 9.0$ Å^{-1}, depending on whether the two beams travel parallel or antiparallel to one another, respectively. Further details of the metastable beam source have been presented in an earlier publication [5]. The scattering chamber is equipped with conventional surface preparation and diagnostic tools, including a crystal cleaver. The sample is mounted on a manipulator with xyz motion and polar and azimuthal rotations. The metastable atom detector consists of a channeltron placed behind an angle-resolving

0031-9007/93/71(8)/1250(4)$06.00

aperture. The size of the beam illuminating the sample and the opening angle of the detector result in an angular resolution of 2.5°. The detector is mounted on a single-axis goniometer that allows rotation in the scattering plane. The detector is insensitive to ground state He atoms and has a very low dark current count rate (<0.05/s).

NiO provides an ideal surface for testing this experimental technique. It is an antiferromagnetic (AF) insulator with a bulk Neél temperature (NT) of ~ 523 K. The cleavage (100) surfaces are chemically more stable than those of the other members of the rock-salt family of AF transition metal oxides. In these crystals, nearest neighbor (nn) Ni ions are coupled ferromagnetically, while next nn Ni ions are AF coupled via superexchange. The latter is an order of magnitude stronger and leads to an overall AF bulk spin ordering that consists of aligned spins in (111) planes which are then AF stacked [6]. If the bulk spin order were extended to the (100) surface, the magnetic unit cell would have a (2×1) structure; see inset of Fig. 1(a). Palmberg, De Wames, and Vredevoe in 1968 reported LEED measurements of half-order peaks for NiO(100) which disappear above the NT, and similar results were subsequently reported [7]. The failure of more recent LEED studies to observe these peaks is probably due to cleavage in air rather than in UHV [8].

The NiO samples were long cleavage rods with a ⟨100⟩ axis. Gold was evaporated onto the sides of the rods in order to reduce charging effects. All He* diffraction measurements were carried out at several angles of incidence with the two beam wave vectors mentioned above, on surfaces cleaved *in situ* at room temperature. The background pressure was better than 1.0×10^{-10} torr, but increased to 1.0×10^{-8} in the presence of the helium beam. The partial pressures of all other residual gases were below 5.0×10^{-11} torr. Monitoring the intensity of the specular beam shows that the cleaved surfaces remain clean for several days. The incident beam intensity was 4×10^{4} counts/s, and the specular beam intensity ~2 counts/s. Scanning times per point were typically 5 min. From our experimental results we estimate the lower bounds of the average local survival probability from the Ni sites to be $\sim0.15\%$ for $k_i=9.0$ Å^{-1} and $\sim0.6\%$ for $k_i=13.6$ Å^{-1}. Diffraction spectra were recorded both along the ⟨10⟩ and along the ⟨11⟩ symmetry directions.

A typical spectrum measured along the ⟨11⟩ direction is shown in Fig. 1(a). The specular peak is clearly visible, and no other diffraction peaks can be discerned. In contrast, the spectra in the ⟨10⟩ direction show appreciable intensities of nonspecular diffraction peaks as shown in Figs. 1(b) and 1(c). For $k_i=13.6$ Å^{-1} strong diffraction peaks are evident that span an angular range well beyond the geometric first-order peak positions [Fig. 1(b)]. For $k_i=9.0$ Å^{-1}, off-specular diffraction peaks appear only in the vicinity of the specular peak and decrease rapidly in amplitude on either side [Fig. 1(c)]. A

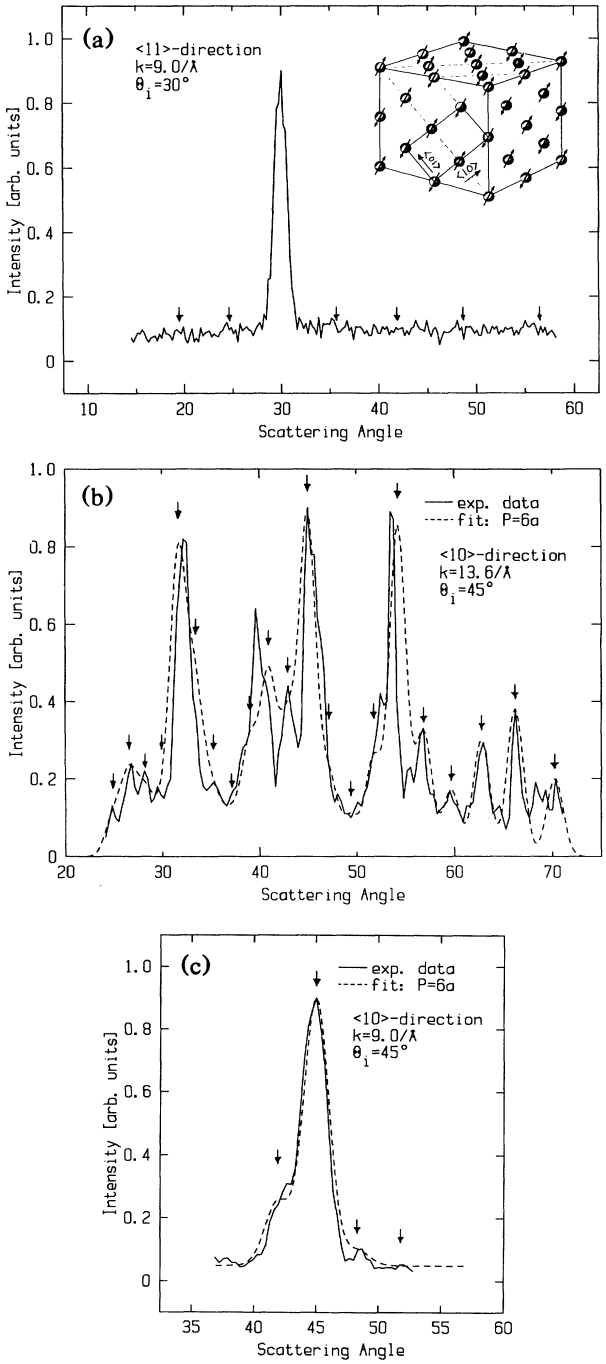

FIG. 1. Observed diffraction spectra. Inset shows the *bulk* magnetic structure. The magnetic unit cell on the (100) surface shows a doubling of the periodicity in the ⟨10⟩ direction. A Gaussian fit with fixed incident beam linewidth was used to determine the periodicity. The peak positions were fixed by the periodicity and only the heights were varied. (a) ⟨11⟩ direction: Only the specular peak is observable. (b) ⟨10⟩ direction: $k=13.6$ Å^{-1}. The Gaussian fit (dashed lines) has a periodicity of 6*a*. Arrows mark the center of the Gaussian peaks. (c) ⟨10⟩ direction: $k=9.0$ Å^{-1}. Note the difference in intensity between the $(-\frac{1}{6},0)$ and $(\frac{1}{6},0)$ diffraction peaks.

persistent feature of all the ⟨10⟩ spectra at $k_i = 9.0$ Å^{-1} is an asymmetry in peak intensity around the specular beam position: Diffraction peaks appearing on the side of the specular beam closer to the surface normal are consistently stronger than those on the other side. This asymmetry is also observed in the ⟨10⟩ spectra at $k_i = 13.6$ Å^{-1} but is less pronounced. The best fit to the measured spectra obtained for both wave vectors at several angles of incidence and from repeated cleaves, yields a superperiodicity of $6a$, where a is the nearest-neighbor distance of Ni atoms on the (100) surface. We were not able to measure diffraction patterns at elevated temperatures because of low count rates and increased noise from the sample heater.

Ground state He diffraction data show that the geometric structure of the NiO(100) surface is not reconstructed [9]. We therefore attribute the superperiodicity of $6a$ to the surface spin configuration. The absence of diffraction peaks other than the specular peak in the ⟨11⟩ direction precludes a (6×6) spin reconstruction. This suggests the presence of a *frozen-spin-wave* (FSW) configuration of the type suggested by Falicov and coworkers for spin ordering on (100) surfaces of MnO-type AF insulators [10]. The bulk AF arrangement leads to two distinct possible orientations of the FSW, directed either along the ⟨10⟩ direction *across* the bulk-ordered (111) plane, or along the ⟨01⟩ direction *within* the (111) planes, as shown in inset in Fig. 1(a).

In order to obtain a better understanding of our results, we have developed a model of the scattering process that includes the effects of a spatially modulated attenuation based on a modified version of the eikonal approximation, together with a hard-corrugated-wall model within the Rayleigh hypothesis. In the conventional version of this formalism, which is widely used in He diffraction model calculations [11], the amplitude in the nth diffraction channel is given by

$$A_n = \frac{1}{\mathcal{A}} \int d\mathbf{R} \exp i[\mathbf{G}_n \cdot \mathbf{R} + (k_{zi} + k_{zn})\zeta(\mathbf{R})] , \qquad (1)$$

where k_{zi} and k_{zn} are the normal components of the incident and scattered wave vectors, $\mathcal{A}$ is the total surface area, $\mathbf{G}_n$ is a surface reciprocal lattice vector, and $\zeta(\mathbf{R})$ is an effective surface corrugation function. In order to account for the attenuation of the scattered metastable beam due to deexcitation to the ground state, we introduce a *complex* corrugation function $\zeta(\mathbf{R}) + i\eta(\mathbf{R})$. While ζ couples to the normal components of the incident and scattered wave vector in the conventional form shown in Eq. (1), the coupling of η has the functional form $(1/k_{zi} + 1/k_{zn})\eta(\mathbf{R})$ expressing the fact that the survival probability is inversely proportional to the normal component of the atom's velocity for both the incoming and outgoing portions of the scattering event: The decay probability increases with the time spent in the "effective decay region." This expression was derived independently by Makoshi using a rigorous time-ordered Green's function approach [12]. The scattered amplitude for a surface wave vector $\mathbf{K}$ then becomes

$$A_{\mathbf{K}} = \frac{1}{\mathcal{A}} \int d\mathbf{R} \exp i\{[\mathbf{K} \cdot \mathbf{R} + (k_{zi} + k_{zn})\zeta(\mathbf{R})] - (1/k_{zi} + 1/k_{zn})\eta(\mathbf{R})\} .$$

$\zeta(\mathbf{R})$ describes the geometric periodicity of the surface structure, and $\eta(\mathbf{R})$ describes the two-dimensional spatially modulated attenuation, reflecting the spin-order periodicity. A detailed study of diffraction spectra based on model calculations incorporating FSW modulations of

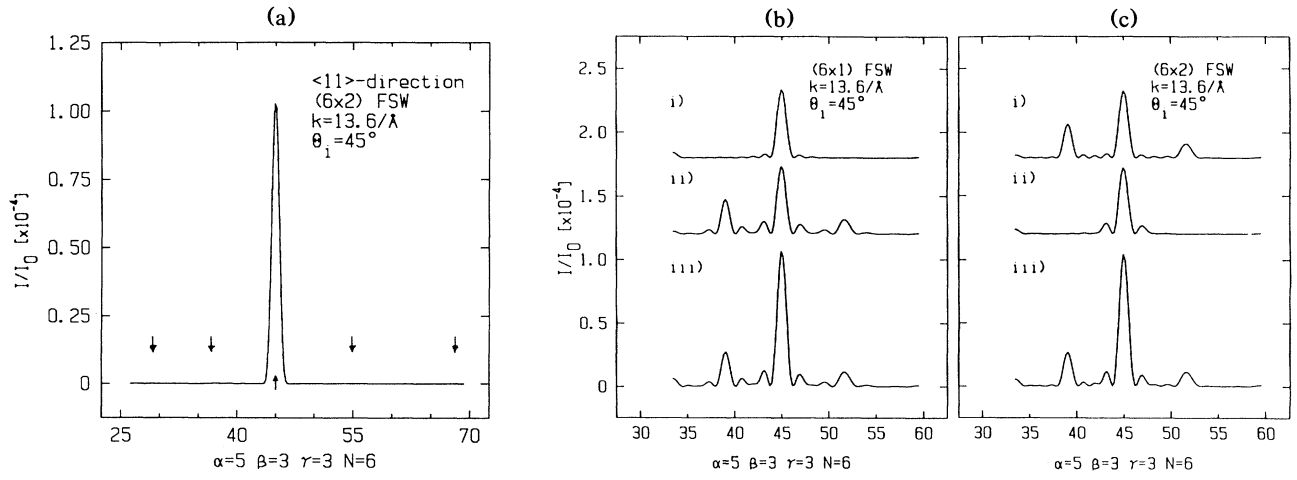

FIG. 2. Calculated diffraction spectra. The corrugation used is 0.1 Å. (a) ⟨11⟩ direction: Only the specular peak is visible, even in the (6×2) configuration where $\frac{1}{2}$-order peaks are anticipated. Arrows mark $\frac{1}{2}$-order positions. Multiple domains add up contributions from both ⟨10⟩ and ⟨01⟩ directions. The resulting spectra look very similar for the two FSW directions. (b) (6×1) configuration. (c) (6×2) configuration (i) ⟨01⟩ direction; (ii) ⟨10⟩ direction; (iii) ⟨01⟩ and ⟨10⟩ directions added.

the form $\eta(\mathbf{R}) = \alpha\{\beta + \gamma\cos^2(\pi X/2a) + \cos^2[\pi Y(X)/6a]\}$ was carried out [13]. α is proportional to the square of the Auger transition matrix element, and the terms inside the brackets comprise the spatial- and spin-dependent electron surface density of states (SDOS) available for the Auger decay channel. A uniform background is expressed by β, γ accounts for the (2×1) contribution, and the last term expresses the FSW contribution. These studies have provided insight into several aspects of the underlying physics of the scattering process: (1) They have revealed a great sensitivity to small modulations in $\eta(\mathbf{R})$ leading to discernible peaks, even in the absence of geometric corrugation. (2) The contribution of $\zeta(\mathbf{R})$ is mainly confined to the intensity of the first order (geometric) peaks. (3) The $1/k_z$ dependence reproduces the observed asymmetry in peak intensities. (4) A (6×2) FSW cannot be ruled out, since the corresponding model calculations, Fig. 2(a), show that the $\frac{1}{2}$-order diffraction peaks expected in the $\langle 11\rangle$ direction are highly attenuated and are not discernible. Moreover, the $\langle 10\rangle$ spectrum, Fig. 2(b), is almost identical to that for the (6×2) pattern, Fig. 2(c). (5) The striking difference between the intensity distribution in the satellite peaks in Figs. 1(b) and 1(c) is attributed to significant changes in the SDOS encountered at the respective wave vectors [14]. This is not surprising since the appreciable difference in the corresponding energies leads to classical turning points that differ by $\sim$0.6 Å.

We do not consider our results to be in contradiction with earlier LEED work [7,8]. The LEED half-order peak intensities are only a few percent of the integral order peaks. The exchange potential associated with a FSW is much weaker and it is likely that the corresponding diffraction peaks could not be observed for that reason. In addition, LEED probes the first few layers of the solid whereas He* probes the tail of the surface charge density.

In conclusion, we have demonstrated a novel experimental technique suitable for exploring long-range antiferromagnetic ordering on magnetic insulators. We have shown that the observed diffraction pattern is a result of a periodic attenuation of the beam due to local spin ordering, rather than due to a spin-spin interaction. Our study of NiO(100) reveals evidence of a frozen spin wave in the $\langle 10\rangle$ direction with a period of $6a$.

This work is supported by U.S. DOE Contract No. DE-FG02-85ER45222.

[1] See, for example, E. Balcar and S. Lovesey, *Theory of Magnetic Neutron and Photon Scattering* (Clarendon, Oxford, 1989), and references therein.
[2] H. D. Hagstrum, in *Inelastic Ion-Surface Collisions*, edited by N. H. Tolk, J. C. Tully, W. Heiland, and C. W. White (Academic, New York, 1977).
[3] H. Conrad, G. Ertl, J. Küppers, W. Sesselmann, B. Woratschek, and H. Haberland, Surf. Sci. **117**, 98 (1982).
[4] See, for example, W. Sesselmann, B. Woratschek, J. Küppers, G. Ertl, and H. Haberland, Phys. Rev. B **35**, 8348 (1987); M. S. Hammond, F. B. Dunning, G. K. Walters, and G. A. Prinz, Phys. Rev. B **45**, 3674 (1992); J. Lee, C. P. Hanrahan, J. Arias, R. M. Martin, and H. Metiu, Phys. Rev. Lett. **51**, 1803 (1983), and references therein.
[5] A. Swan, W. Franzen, M. El-Batanouny, and K. M. Martini, Mat. Res. Soc. Symp. Proc. **208**, 273 (1991).
[6] W. L. Roth, J. Appl. Phys. **31**, 2000 (1960).
[7] P. W. Palmberg, R. E. De Wames, and L. A. Vredevoe, Phys. Rev. Lett. **21**, 682 (1968).
[8] T. Suzuki, N. Hirota, H. Tanaka, and H. Watanabe, J. Phys. Soc. Jpn. **30**, 888 (1971); M. Prutton, J. Phys. C **8**, 2401 (1975); B. Sinkovic (private communication).
[9] W. P. Brug, G. Chern, J. Duan, G. G. Bishop, S. A. Safron, and J. G. Scofronick, J. Vac. Sci. Technol. A **10**, 2222 (1992); P. Toennies (private communication).
[10] D. C. Chrzan and L. M. Falicov, Phys. Rev. B **39**, 3159 (1989).
[11] See, for example, T. Engel, and K. H. Rieder, *Structural Studies of Surfaces* (Springer-Verlag, Berlin, 1982).
[12] K. Makoshi, Surf. Sci. **254**, 281 (1991).
[13] No attempts were made to fit to experimental data.
[14] A. Swan *et al.* (to be published).